CENTRE DE RECERCA MATEMÀTICA

Preprint núm. 1153
April 2013

Modelling the solidification of a power-law fluid flowing through a narrow pipe

T.G. Myers, J. Low

MODELLING THE SOLIDIFICATION OF A POWER-LAW FLUID FLOWING THROUGH A NARROW PIPE

T. G. MYERS AND J. LOW

Abstract. We develop a mathematical model to simulate the solidification process of a non-Newtonian power-law fluid flowing through a circular cross-section microchannel. The initial system consists of three partial differential equations, describing the fluid flow and temperature in the liquid and solid, which are solved over a domain specified by the Stefan condition. This is reduced to solving a partially coupled system consisting of a single partial differential equation and the Stefan condition. Results show qualitative differences, depending on the power law index and imposed flow conditions, between Newtonian and non-Newtonian solidification. The model behaviour is illustrated using power law models for blood and polyethylene oxide.

1. Introduction

Solidification of fluid flowing through a pipe is a classical problem motivated by, for example, the damage caused as water expands upon freezing or the development of lava tubes [1, 2]. Recently interest has been stimulated by applications on the micro and nano-scales. One such application arises due to the difficulties of manufacturing valves suitable for use in micro-channels since these obviously occupy space and induce flow resistance (the difficulties are discussed in detail in [3, 4]). To avoid the issue of miniaturization of valves researchers have come up with a variety of new techniques, one of these being the phase change valve, where an external cooling system acts to freeze the fluid within the channel. The idea was first proposed by Bevan and Mutton, see [5, 6] and extended by numerous research groups, see for example the review of [4]. This form of valve is particularly useful when rapid closure is not essential, such as in micro-PCR chips, liquid chromatography and electrophoresis. In the field of cryopreservation a standard technique involves solidifying a fluid-cell mixture contained within a tube which is then immersed in liquid nitrogen. Understanding the solidification process is an important step towards minimising cell damage [7, 8].

Mathematical models of solidification in small channels invariably deal with Newtonian fluids. In practice most industrial and biological fluids are non-Newtonian and so there is a clear need to extend the scope of these studies to incorporate such fluids. This is the purpose of the present paper.

Key words and phrases. Stefan problem, Power-law fluid, Microchannel flow, Phase change, Phase change valve, Cryopreservation.

2. Mathematical Model

The equations describing the laminar flow of an incompressible power law fluid in a circular cross-section pipe of radius R are well-known:

$$\rho_l \frac{d\mathbf{u}}{dt} = -\nabla p + \nabla \cdot \boldsymbol{\sigma} \qquad \nabla \cdot \mathbf{u} = 0\,, \tag{1}$$

where ρ denotes the density, $\mathbf{u}$ the velocity, p the pressure and $\boldsymbol{\sigma}$ the stress tensor.

When the flow is primarily directed in the axial direction we may neglect all terms in the stress tensor, with the exception $\sigma_{xr} = m(-u_r)^{n-1}$, where m is the consistency and n the power law index. The minus sign is employed since the velocity gradient, u_r, is negative, see [9, 10]. To describe solidification these equations must be coupled to the thermal problem

$$\frac{\partial T}{\partial t} + \mathbf{u} \cdot \nabla T = \alpha_l \nabla^2 T \qquad 0 < r < h(x,t) \tag{2}$$

$$\frac{\partial \theta}{\partial t} = \alpha_s \nabla^2 \theta \qquad h(x,t) < r < R \tag{3}$$

where T, θ are the liquid and solid temperatures and α is the thermal diffusivity. The position of the solidification front, $r = h(x,t)$, is determined through the Stefan condition

$$\rho_s L_f \frac{dh}{dt} = k_s \left.\frac{\partial \theta}{\partial r}\right|_{r=h} - k_l \left.\frac{\partial T}{\partial r}\right|_{r=h}\,. \tag{4}$$

The problem configuration is shown on Figure 1.

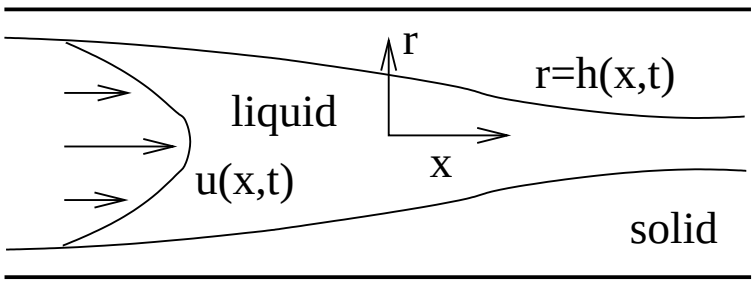

Figure 1. Problem configuration.

With the exception of the power law stress tensor, the above equations are identical to those describing the solidification of a Newtonian fluid studied in [11] (which in turn were adapted from the models in [12, 13]). In [11] the governing equations were non-dimensionalised in the standard manner consistent with lubrication theory. Obviously we may also non-dimensionalise the above system, however, if the flow is driven by a pressure gradient (and so Δp is fixed) then the velocity scale depends on the power law parameters. Specifically, with a Newtonian fluid $U = (R^2 \Delta p/\mu L)$ but with a power-law fluid, $U = (R^{n+1}\Delta p/mL)^{1/n}$.

This means that when we compare results for different fluids, with different values of n, then the definition of the velocity scale changes and so the comparisons are not appropriate. For example in [11] the pipe closure time was plotted against the Péclet number, $Pe = UR^2/(\alpha_l L)$. With a power law fluid, if the definition of U changes with each fluid then so will the definition of Pe. For this reason we will work in dimensional form, whilst retaining the approximations suggested from the earlier non-dimensional study.

Firstly, we simplify the flow equations in line with lubrication theory, which requires a small aspect ratio and small reduced Reynolds number (the aspect ratio squared multiplied by the Reynolds number) [14]. Consequently, the flow is described by

$$-\frac{m}{r}\frac{\partial}{\partial r}\left(r\left(-\frac{\partial u}{\partial r}\right)^n\right) \approx \frac{\partial p}{\partial x}, \qquad \frac{\partial p}{\partial r} \approx 0, \qquad \frac{\partial u}{\partial x} + \frac{1}{r}\frac{\partial}{\partial r}(rw) = 0. \tag{5}$$

These equations are subject to no-slip and a momentum balance at the solidification front and symmetry at the centre-line, see [11]

$$u(x, h(x,t), t) = 0, \quad w(x,h,t) = \left(1 - \frac{\rho_s}{\rho_l}\right)\frac{\partial h}{\partial t}, \tag{6}$$

$$\left.\frac{\partial u}{\partial r}\right|_{r=0} = 0, \quad w(x,0,t) = 0. \tag{7}$$

Equation (5b) indicates $p = p(x,t)$. This allows Eq. (5a) to be integrated

$$u = \left[\frac{1}{2m}\left(-\frac{\partial p}{\partial x}\right)\right]^{1/n}\left(\frac{n}{n+1}\right)\left[h^{\frac{n+1}{n}} - r^{\frac{n+1}{n}}\right]. \tag{8}$$

Since the aim of this study is to determine when the flow is stopped the flux is an important quantity

$$Q = 2\pi\int_0^h ur\ \mathrm{d}r = \pi\left(\frac{n}{3n+1}\right)\left[\frac{1}{2m}\left(-\frac{\partial p}{\partial x}\right)\right]^{1/n} h^{\frac{3n+1}{n}}. \tag{9}$$

Since the fluid is incompressible $Q = Q(t)$ and so Eq. (9) allows us to determine the pressure gradient in terms of the flux and position of the solidification front. This permits the removal of the pressure gradient from the velocity expression

$$u = \frac{Q}{\pi h^2}\left(\frac{3n+1}{n+1}\right)\left[1 - \left(\frac{r}{h}\right)^{\frac{n+1}{n}}\right]. \tag{10}$$

Integrating Eq. (9) we may write the pressure drop along the pipe as

$$\Delta p = p_{\text{in}} - p_{\text{out}} = 2m\left(\frac{Q}{\pi}\left[\frac{3n+1}{n}\right]\right)^n \int_0^L \frac{1}{h^{3n+1}}\ \mathrm{d}x\,. \tag{11}$$

CRM Preprint Series number 1153

The incompressibility condition, Eq. (5c), then gives the velocity in the radial direction

$$w = -\frac{1}{r}\frac{\partial}{\partial x}\left\{\frac{Q}{\pi h^2}\left(\frac{3n+1}{n+1}\right)\left[\frac{r^2}{2}-\frac{n}{3n+1}\frac{r^{(3n+1)/n}}{h^{(n+1)/n}}\right]\right\}. \tag{12}$$

The equivalent Newtonian expression may be retrieved from the above equations by setting $n = 1$, see [10, 11].

Before moving on to the thermal problem we make a change of co-ordinate by defining $\hat{r} = r/h$. This fixes the boundary of the flow domain to $\hat{r} \in [0, 1]$. Noting that $\hat{r}_x = -h_x\hat{r}/h$ we may write

$$w = -\frac{Q}{\pi}\left(\frac{3n+1}{n+1}\right)\frac{1}{r}\frac{\partial}{\partial x}\left\{\left[\frac{\hat{r}^2}{2}-\frac{n}{3n+1}\hat{r}^{(3n+1)/n}\right]\right\} = \hat{r}h_x u\,. \tag{13}$$

As will be seen, this significantly simplifies the thermal problem.

Under the same restrictions as applied to the flow equations the thermal problem reduces to

$$\left(u\frac{\partial T}{\partial x}+w\frac{\partial T}{\partial r}\right) = \frac{\alpha_l}{r}\frac{\partial}{\partial r}\left(r\frac{\partial T}{\partial r}\right), \qquad \frac{1}{r}\frac{\partial}{\partial r}\left(r\frac{\partial \theta}{\partial r}\right) = 0 \tag{14}$$

subject to

$$\theta|_{r=R} = T_w, \qquad \theta|_{r=h} = T|_{r=h} = T_f, \qquad \left.\frac{\partial T}{\partial r}\right|_{r=0} = 0, \qquad T|_{x=0} = T_0\,. \tag{15}$$

Hence

$$\theta = T_f + \frac{T_w - T_f}{\ln(R/h)}\ln\hat{r}\,. \tag{16}$$

In terms of the new radial co-ordinate the liquid temperature $T(r, x, t) = T(x, \hat{r}(x, r, t), t)$ is described by

$$\left(u\left[\frac{\partial T}{\partial x}-\frac{h_x\hat{r}}{h}\frac{\partial T}{\partial \hat{r}}\right]+\frac{h_x\hat{r}u}{h}\frac{\partial T}{\partial \hat{r}}\right) = u\frac{\partial T}{\partial x} = \frac{\alpha_l}{h^2}\frac{1}{\hat{r}}\frac{\partial}{\partial \hat{r}}\left(\hat{r}\frac{\partial T}{\partial \hat{r}}\right). \tag{17}$$

Substituting for the liquid velocity, via Eq. (10), leads to a separable equation for T

$$\frac{Q}{\pi}\left(\frac{3n+1}{n+1}\right)\left(1-\hat{r}^{\frac{n+1}{n}}\right)\frac{\partial T}{\partial x} = \frac{\alpha_l}{\hat{r}}\frac{\partial}{\partial \hat{r}}\left(\hat{r}\frac{\partial T}{\partial \hat{r}}\right). \tag{18}$$

This is a good time to highlight the importance of the new co-ordinate $\hat{r}$. The position of the solidification front $r = h(x, t)$ is still unknown and determined by the Stefan condition (4). If we work in terms of r then the liquid temperature involves both velocities u, w and is applied over the unknown domain $r \in [0, h]$. The Stefan condition is then coupled to the flow problem and the two equations must be solved in parallel. Working in terms of $\hat{r}$ the liquid temperature equation,

Eq. (18), is independent of h and so may be solved independently. Once this is done the temperature gradient may be substituted into the Stefan condition

$$\rho_s L_f h \frac{dh}{dt} = k_s \left.\frac{\partial \theta}{\partial \hat{r}}\right|_{\hat{r}=1} - k_l \left.\frac{\partial T}{\partial \hat{r}}\right|_{\hat{r}=1} \tag{19}$$

to determine $h(x,t)$.

Property [units]	Blood	Polyethylene Oxide
Power-Law index n	0.6	0.4133
Fluid Consistency m [Pa s^n]	0.035	13.787
Melting Temperature T_f [°C]	-0.3	63
Liquid Density ρ_l [kg/m^3]	1060	1130
Latent Heat of Fusion L_f [J/ kg]	3.15×10^5	3.8×10^5
Specific Heat Capacity c_p [J/ kg K]	3594	2040
Solid Thermal Conductivity k_s [W/mK]	1.589	0.17
Liquid Thermal Conductivity k_l [W/mK]	0.492	0.0525 (*)
Liquid Thermal Diffusivity $\alpha_l = k_l/(\rho_l c_p)$ [m^2/s]	1.29×10^{-7}	2.2×10^{-8}

TABLE 1. *Fluid properties taken from various sources* [10, 15, 16, 17, 18, 19, 20, 21]. *(*) Calculated from k_s by using the same ratio of k_l/k_s as that for blood.*

3. Results

The initially complex problem of solving the flow and heat equations (1–3) over a domain specified by the Stefan condition (4) has been reduced to solving two simple equations (18,19). Equation (18) may be solved analytically for certain values of n but in general there is no closed form solution, hence we now seek a numerical solution. Our scheme begins with a clean channel, $h = R$ and the initial flux $Q(0)$ is determined in terms of the specified pressure drop via equation (11). The flux $Q(0)$ is then substituted into the heat equation, Eq. (18)

CRM Preprint Series number 1153

which is solved using Matlab routine PDEPE, subject to the appropriate boundary conditions specified in equation (15), to determine the liquid temperature T. This also outputs the gradient $T_{\hat{r}}$ required for the Stefan condition. The derivative of equation (16) provides $\theta_{\hat{r}}$ and so we may integrate the Stefan condition, Eq. (19), to update $h(x,t)$. The flux is then recalculated and the process continued until $h = 0$ at some point. We now illustrate the solutions obtained through this process via two examples, using parameter values appropriate for blood and polyethylene oxide (PEO). The fluid parameter values, taken from a variety of sources [10, 15, 16, 17, 18, 19, 20, 21], are given in Table 1. The exception being the thermal conductivity of liquid PEO, which we were unable to find. Instead we used the ratio for k_l/k_s for blood to calculate k_l for PEO. For all the results, we take the length of the microchannel length to be 10cm and the radius as 1mm.

In Fig. 2 we show the evolution of a solidification front for blood flowing through a cooled pipe. The solid lines indicate the movement using a non-Newtonian model whilst the dashed lines demonstrate how solidification would progress with an equivalent Newtonian fluid. The Newtonian equivalent is chosen such that the initial flux is the same as the non-Newtonian model. According to Eq. (9), the initial Newtonian and non-Newtonian fluxes match when

$$\mu = \left(\frac{3n+1}{8n}\right)(2m)^{1/n} R^{(n-1)/n}(-p_x)^{(n-1)/n} \ . \tag{20}$$

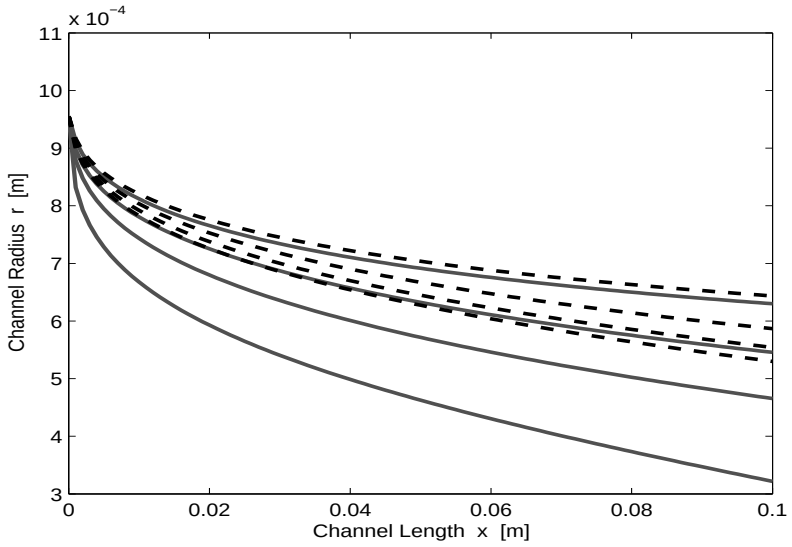

FIGURE 2. The position of the solidification fronts for blood at times $t =$ 9.9, 20.5, 31.1, 41.7s. The solid lines represent the non-Newtonian model, the dashed lines are the equivalent Newtonian case.

Note that the Newtonian flux is obtained by setting $h = R$, $n = 1$ and $m = \mu$ in Eq. (9). The results are obtained using parameter values given in Table 1 and

with a pressure drop along the channel of 1.36×10^3 Pa, corresponding to an initial flux of 4.4×10^{-6} m^{3}s^{-1}, and $T_0 = 9.3°$C, $T_f = -0.3°$C, $T_w = -3.27°$C at times $t = 9.9, 20.5, 31.1, 41.7$s. The equivalent Newtonian viscosity from Eq. (20) is 0.0012 Pa s. At early times both fluid models show similar solidification rates, however as time proceeds the non-Newtonian model starts to solidify more rapidly. This result appears counter-intuitive since in [11] it is shown that faster flows lead to slower solidification and one would expect a shear thinning fluid to flow faster than an equivalent Newtonian fluid. The problem may be traced to the lack of realism of the power-law model near the central region, where $u_r \to 0$. As the velocity gradient tends to zero the viscosity ($\propto u_r^{n-1}$) tends to infinity and so acts to slow down the fluid. Hence for a fixed pressure gradient the shear thinning fluid can in fact flow more slowly than a Newtonian counterpart and so solidify more rapidly. This problem with the power law model is discussed in detail in [10, 22].

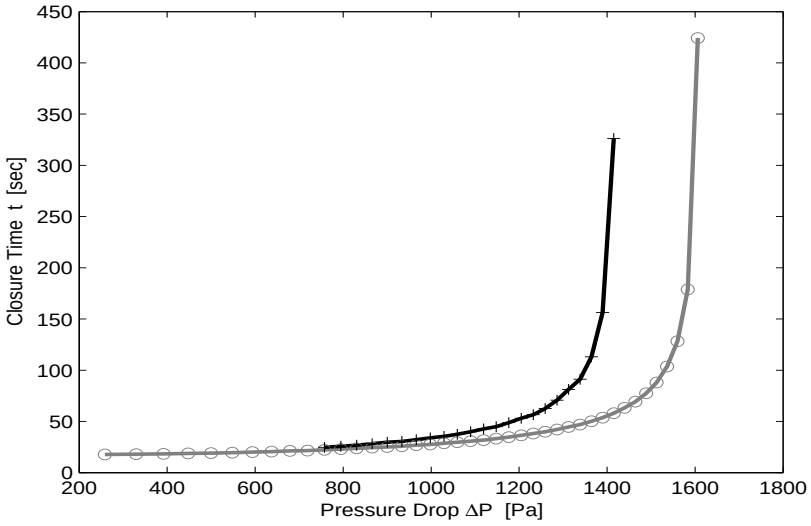

FIGURE 3. The closure time against the imposed pressure drop across the channel for blood when $T_0 = 9.3°$C, $T_f = -0.3°$C and $T_w = -3.27°$C. Circles points are those for the non-Newtonian case, whilst the cross points correspond to the equivalent Newtonian case. The lines are for guidance.

In Fig. 3 we plot the closure time against pressure drop for both non-Newtonian and Newtonian blood. Increasing the pressure drop leads to an increase in flow rate which slows down the solidification process until eventually a stage is reached where closure no longer occurs. In this example, for the non-Newtonian case, we find the channel no longer closes when $\Delta p > 1600$Pa. For the case shown in Fig. 2, with $\Delta p = 1.36 \times 10^3$ we see closure will occur for $t \approx 50$s. The equivalent Newtonian graph takes the same qualitative form as that of its non-Newtonian

counterpart. For low pressure drops the curves are identical, for larger values Newtonian closure is slower for a given pressure drop and the critical pressure drop is reduced to around 1415 Pa.

In the analysis of [11] it is shown that the closure time for relatively low pressure drops (well below the critical value) is controlled through conduction: advection only becomes important as the pressure drop increases. In Figure 3 this may be observed through the approximately constant value of the closure time for $\Delta P < 800$ Pa. The subsequent increase in closure time reflects the increasing importance of advection as ΔP grows. For the constant closure time region, a time-scale for solidification may be obtained from the Stefan condition, Eq. (4),

$$\tau = \rho_s L_f R^2/(k_s \Delta T) \tag{21}$$

where the temperature scale $\Delta T = T_0 - T_w$ denotes the temperature change between the wall and incoming fluid (note, in [11] ΔT is incorrectly written as $T_f - T_w$). The factors affecting solidification are then easy to read off: for a given fluid the solidification time increases proportional to R^2 or $(T_0 - T_w)^{-1}$. Taking values from Table 1 (we assume that $\rho_s = \rho_l$) we find that for blood the closure time $\tau \approx 2.1 \times 10^8 R^2/\Delta T$ and specifically for the current problem, with $R = 1$mm, $T_0 - T_w = 9.6°$C we find $\tau \approx 16.7$s. The minimum time on Figure 3 is around 17s.

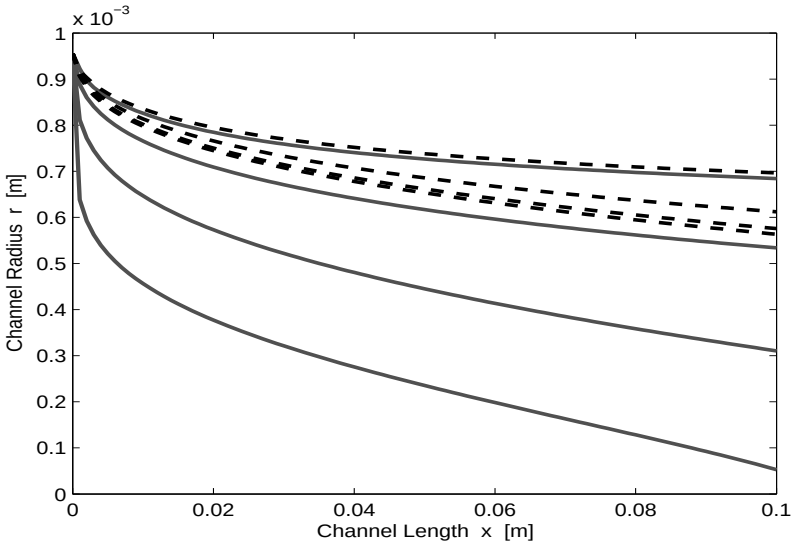

FIGURE 4. The position of the solidification fronts for PEO at times $t =$ 57.3, 118.1, 319.0, 384.4s. The solid lines represent the non-Newtonian model, the dashed lines are the equivalent Newtonian case.

In Fig. 4 we show solidification curves at times $t = 57.3$, 118.1, 319.0, 384.4s for PEO subject to a pressure drop 5.41×10^4 Pa (and so an initial flux $Q(0) =$

7.8×10^{-7} m^{3}s^{-1}), $T_0 = 73°$C, $T_f = 63°$C, $T_w = 59.9°$C and equivalent Newtonian viscosity $\mu = 0.2738$ Pa s. Since the viscosity of PEO is much greater than that of blood significantly higher pressures are required to drive the flow. However, the greater solidification times when compared to blood are primarily due to the decrease in thermal conductivity. This is clear from Eq. (21), where τ is proportional to the inverse of k_s: PEO has a k_s value ten times lower than that of blood. Qualitatively the results are similar to those shown in Fig. 2 in that the non-Newtonian model shows faster solidification than the equivalent Newtonian fluid. The closure time against pressure drop is shown in Fig. 5. The critical pressure drop, beyond which closure will not occur, is around $\Delta p = 6.06\times10^4, 5.5\times10^4$Pa for the non-Newtonian and Newtonian models respectively. We can see that for the example of Figure 4 we expect the non-Newtonian model to exhibit closure at around $\tau = 400$s whilst the Newtonian model has $\tau \approx 1600$s.

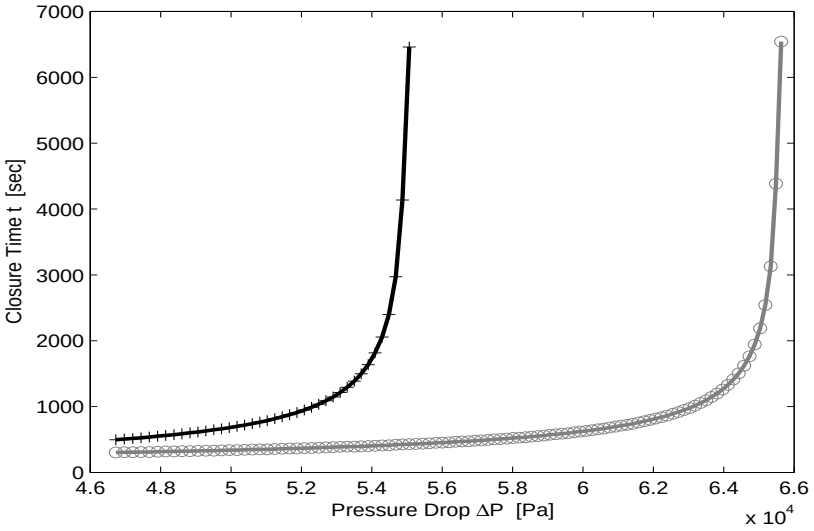

FIGURE 5. The closure time against the imposed pressure drop across the channel for Polyethylene oxide when $T_0 = 73°$C, $T_f = 63°$C and $T_w = 59.9°$C. The circle points correspond to the non-Newtonian case whilst the crosses are those for the Newtonian and the lines are for guidance.

The solidification curves shown in Figs. 2 and 4 were deliberately chosen to highlight differences in the models and so both examples use a Δp close to the critical value for the Newtonian fluid. Hence they show a similar solution form in that the solidification fronts show an approximately linear decrease away from the entrance region. However, if we decrease Δp then the solutions will start to coincide. The Newtonian analysis of [11] shows that at sufficiently low Δp the profiles become flat away from the entrance, and obviously since the models coincide for low pressure drop this result will hold for non-Newtonian liquids. This

CRM Preprint Series number 1153

has important implications for cryopreservation. If the profile is linear when the flow is stopped then there will be a significant amount of trapped fluid which may subsequently expand on freezing and so add stress to the system. A flat profile will have a relatively small amount of trapped fluid, leading to a lower stress system.

4. Conclusion

We have derived a mathematical model to describe the solidification of a power-law fluid inside a narrow channel and solved the model equations using MATLAB. Taking blood and polyethylene oxide as examples, we find that in general the shear thinning fluid freezes faster than the Newtonian equivalent under the same pressure drop. This change in rate may be due to two causes, firstly there is the well-known inadequacy of the power law model: a shear thinning fluid in fact has an infinite viscosity along the flow centre-line and the increased viscosity in this region acts to slow the fluid down, so leading to more rapid freezing. Secondly, it is difficult to prescribe an equivalent Newtonian fluid: here we have chosen a Newtonian viscosity that provides the same initial flux as the power law fluid, but as the flux decreases this chosen viscosity will diverge from the average non-Newtonian viscosity and so the models may not be equivalent. In general, for low flow rates or equivalently low pressure drops the solidification time was shown to be independent of the flow rate. Beyond a certain point increasing the flow rate increases the solidification time. A decrease in the power law index $n < 1$ will decrease the solidification time.

Both Newtonian and non-Newtonian fluids show a critical pressure drop, above which the flow will never completely stop. The value of the pressure drop increases with decreasing power law index. The solidification profile is also affected by the pressure drop: for low pressure drops the front is approximately flat, for higher values there is a linear decrease. This has significant consequences for phase change valves or cryopreservation if the fluid expands on freezing. A flat profile will stop flow with little liquid in the frozen region and so little subsequent thermal expansion. However a linear profile will leave a high proportion of liquid when flow stops which may then expand and damage equipment or cells. For this point of view the flat profile is clearly most desirable.

Acknowledgements

TM gratefully acknowledges the support of this research through the Marie Curie International Reintegration Grant *Industrial applications of moving boundary problems*, grant No. FP7-256417 and Ministerio de Ciencia e Innovación grant MTM2011-23789. JL acknowledges post-doctoral funding through the Centre de Recerca de Matemàtica.

References

[1] J.R. Lister, P.J. Dellar, Solidification of pressure-driven flow in a finite rigid channel with application to volcanic eruptions, Journal of Fluid Mechanics **323** (1996), 267–283.

[2] B. Weigand, J. Braun, S.O. Neumann, K.J. Rinck, Freezing in forced convection flows inside ducts: A review, Heat and Mass Transfer **32** (1997), 341–351.

[3] M.J. Felton, The new generation of microvalves, Analytical Chemistry **75** (2003), no. 19, 429A–432A.

[4] C. Zhang, D. Xing, Y. Li, Micropumps, microvalves, and micromixers within PCR microfluidic chips: Advances and trends, Biotechnolgy Advances **25** (2007), 483–514.

[5] C.D. Bevan, I.M. Mutton, Freeze-thaw flow management: a novel concept for high performance liquid chromatography, capillary electrophoresis, electrochromatography and associated techniques, Journal of Chromatography A **697** (1995), 541–548.

[6] C.D. Bevan, I.M. Mutton, Use of Freeze-Thaw Flow Controlling and Switching Tubes, Analytical Chemistry 67 (1995), 1470-1473.

[7] Y.S. Song, S.J. Moon L. Hulli, S.K. Hasan, E. Kayaalp, U. Demirci, Microfluidics for cryopreservation, Lab Chip 9 (2009) 1874-1881, DOI:10.1039/b823062e.

[8] F. Xu, S.J. Moon, X. Zhang, L. Shao, Y.S. Song, U. Demirci, Multi-scale heat and mass transfer modelling of cell and tissue cryopreservation. Phil. Trans. R. Soc. A **368** (2010), 561–583. DOI:10.1098/rsta.2009.0248.

[9] R.P. Chhabra, J.F. Richardson, Non-Newtonian Flow and Applied Rheology, second ed., Butterworth-Heinemann, 2008.

[10] T.G. Myers, Application of non-Newtonian Models to Thin Film Flow, Physical Review E **72** (2005), 066302.

[11] T.G. Myers, J. Low, An Approximate Mathematical Model for Solidification of a Flowing Liquid in a Microchannel, Microfluidics and Nanofluidics (2011), DOI:10.1007/s10404-011-0807-4.

[12] T.G. Myers, J.P.F. Charpin, C.P. Thompson, Slowly accreting ice due to supercooled water impacting on a cold surface, Physics of Fluids **14(1)** (2002), no. 1, 240.

[13] T.G. Myers, J.P.F. Charpin, S.J. Chapman, The flow and solidification of a thin fluid film on an arbitrary three-dimensional surface. Physics of Fluids **14** (2002), no. 8, 2788–2803.

[14] H. Ockendon, J.R. Ockendon, Viscous Flows, Cambridge University Press, 1995.

[15] Y. Rabin, The Effect Of Temperature-Dependent Thermal Conductivity in Heat Transfer Simulations of Frozen Biomaterials, Cryo Letters **21** (2000), no. (3), 163–170.

[16] J.D. Cutnell, K.W. Johnson, Physics, fourth ed., Wiley, 1998, pp. 308.

[17] T.A. Balasubramaniam, H.F. Bowman, Thermal Conductivity and Thermal Diffusivity of Biomaterials: A Simultaneous Measurement Technique, Journal of Biomechanical Engineering **99** (1997), 148.

[18] A.S.T. Blake, G.W. Petley, C.D. Deakin, Effects of changes in packed cell volume on the specific heat capacity of blood: implications for studies measuring heat exchange in extracorporeal circuits, British Journal of Anaesthesia **84(1)** (2000), 28–32.

[19] J.G. Eftekhar, Some Thermophysical Properties of Blood Components and Coolants for Frozen Blood Shipping Containers, PhD Thesis, The University of Texas at San Antonio, TX, 1989, http://handle.dtic.mil/100.2/ADA216099.Lastaccessed28-06-2011.

[20] Wolfram Mathematica ChemicalData via. Wolfram|Alpha, http://www.wolframalpha.com/input/?i=polyethylene+oxide.Lastaccessed29-06-2011.

[21] S. Maity, L.N. Downen, J.R. Bochinski, L.I. Clarke, Embedded metal nanoparticles as localized heat sources: An alternative processing approach for complex polymeric materials, Polymer **52** (2011), 1674–1685.

CRM Preprint Series number 1153

[22] J.P.F. Charpin, M. Lombe and T.G. Myers, Spin coating of non-Newtonian fluids with a moving front. Phys. Rev E **76** (2007), 016312. DOI:10.1103/PhysRevE.76.016312.

T. G. Myers
Centre de Recerca Matemàtica
Campus de Bellaterra, Edifici C
08193 Bellaterra (Barcelona), Spain
Tel: +34 93 581 1081
Fax: +34 93 581 2202
E-mail address: tmyers@crm.cat

J. Low

CRM
CENTRE DE RECERCA MATEMÀTICA
Facultat de Ciències, UAB
08193 Bellaterra
Barcelona, Spain
www.crm.cat